

## CFD MODELLING OF BUOYANCY-DRIVEN NATURAL VENTILATION OPPOSED BY WIND

Malcolm Cook<sup>1</sup>, Yingchun Ji<sup>1</sup> and Gary Hunt<sup>2</sup>

<sup>1</sup> Institute of Energy and Sustainable Development, De Montfort University, Leicester,  
LE1 9BH, UK

<sup>2</sup> Department of Civil and Environmental Engineering,  
Imperial College London, London, SW7 2AZ, UK

### ABSTRACT

This paper presents CFD simulations of natural displacement ventilation airflows in which the buoyancy force produced by a heat source is opposed by a wind force. Cases investigated focus on wind-buoyancy force relationships for which a two-layer stratification is maintained. CFD predictions of the position of the interface separating the two layers and the change in reduced gravity (temperature difference) between them are compared with the analytical work and salt-bath measurements of Hunt and Linden (2000, 2005). Comparisons are good with only minor discrepancies in the interface position and a small under-prediction of the upper layer reduced gravity.

### INTRODUCTION

Computational fluid dynamics (CFD) simulation is increasingly being used to guide the development of natural ventilation strategies in low-energy building designs. This is partly attributable to a renewed interest in natural ventilation, but also due to the availability of powerful affordable desk-top computers which are able to solve the complex non-linear equations in CFD models within an acceptable time frame.

Recent work by Cook (1998), Cook and Lomas (1998) and Cook et al. (2003) has examined the application of CFD to predict passive airflows in buildings driven by internal heat sources and more recently assisting wind flows. The aims of this work have been to benchmark the CFD models through validation by comparison with analytical predictions of these flows (e.g. Linden et al. (1990), Hunt and Linden (2000, 2001, 2005)) and experimental data taken from their laboratory measurements. This benchmarking has proved successful and, thus, in addition to capturing the bulk features of the flow and confirming the governing flow parameters as identified by the analytical modelling, the CFD then offers a convenient means for predicting, for example, the detailed spatial variation of flow parameters such as air speed and temperature which may be crucial for comfort analysis and detailed design in more complex spaces.

Very little information is available offering guidelines on how best to use CFD for modeling natural ventilation. The work reported herein is part of an EPSRC supported project (GR/N37346), the aim of which is to begin developing such guidelines.

The work in this paper builds on previous work by the authors. Cook (1998) and Cook and Lomas (1998) investigated steady natural displacement ventilation in a single space driven by buoyancy alone. These simulations used an external flow domain which enabled the airflow through the inlets and outlets to be modelled explicitly without the need for boundary conditions at these locations. Results agreed favourably with analytical predictions and experimental measurements of Linden et al. (1990). The work compared predictions using the standard  $k-\epsilon$  turbulence model of Launder and Spalding (1974) with the Renormalisation Group (RNG)  $k-\epsilon$  turbulence model developed by Yakhot et al. (1992). These comparisons showed that the RNG model gave results closer to the analytical and experimental work due to a lower rate of entrainment into the plume. Using some of the techniques developed in this work, simulations were conducted for a wind assisted buoyancy-driven displacement ventilation flow (Cook et al. 2003) and compared with analytical work (Hunt and Linden 2001). A fundamental difference in the way these simulations were modelled relative to those reported in Cook and Lomas (1998) was the use of boundary conditions specified directly at the openings which considerably reduced the amount of computation necessary. Results were again very encouraging with only minor discrepancies observed between predictions and measurements.

The simulations reported in this paper are for natural displacement ventilation in which wind forces oppose buoyancy. Predictions of the key features of the flow are compared with the analytical and experimental work carried out by Hunt and Linden (2000, 2005).

The paper comprises the following sections: *analytical and experimental work* in which the work of Hunt and Linden (2000, 2005) is summarised; *simulation details*, where the cases investigated are

defined and the CFD model presented; *discussion and results analysis*; and *conclusions*.

## ANALYTICAL AND EXPERIMENTAL WORK

Hunt and Linden (2000, 2005) consider the steady airflow and thermal stratification within a highly-insulated enclosure containing a point heat source in the centre of the floor with openings to the exterior air at high- and low-level (Figure 1). The upper opening is in a region of (relatively) positive wind pressure and the lower opening in a region of (relatively) negative wind pressure.

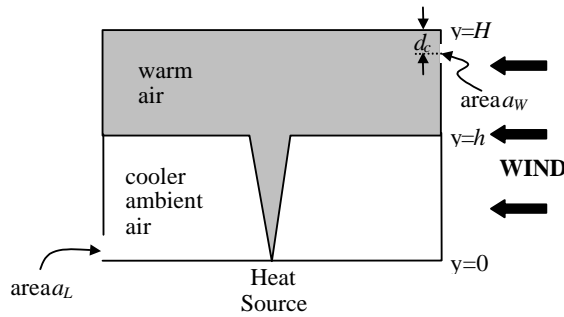


Figure 1 Natural displacement ventilation in a space containing a point heat source

In the absence of wind, Linden et al. (1990) show that warm air rising as a turbulent plume above the heat source stratifies the interior air into two homogenous layers – a warm upper and cooler lower layer. The warm upper layer drives flow out through the high-level opening(s) which is replenished by air at ambient temperature entering the space at low-level. In this buoyancy-driven flow, a stable stratification is established in which the height of the interface,  $h$ , between the warm and ambient air layers can be expressed as a function  $a_w$ ,  $a_L$ , and  $H$ . A wind acting on the upper opening (from the right in Figure 1) serves to oppose the buoyancy-driven flow. Hunt and Linden (2000, 2005), referred to hereafter as HL, show that in this case, multiple-steady flow solutions are possible for a range of identical enclosure geometries, wind speeds and heat loads. The two stable steady flows (mixing and displacement ventilation) that are possible represent extremes of ventilation strategy and reversals in flow direction through the enclosure.

The simulations discussed and presented in this paper are concerned with a range of ‘weak’ opposing winds for which the general two-layer stratification shown in figure 1 is maintained. Under these conditions, the leeward opening behaves as an inlet and the windward opening as an outlet. For this displacement flow case, HL derived the following analytical model for predicting the interface height,  $h$ .

$$\frac{A^*}{H^2} = \frac{C^{3/2} \xi^{5/3}}{\left( (1 - \xi - d_c/H) / \xi^{5/3} - C Fr^2 \right)^{1/2}} \quad (1)$$

where  $A^*$  is an effective opening area given by

$$\frac{A^*}{H^2} = \frac{a_w a_L}{H^2} \left( \frac{2C_e^2 C_d^2}{C_d^2 a_w^2 + C_e^2 a_L^2} \right)^{1/2} \quad (2)$$

and where

$$Fr = \frac{(\Delta\rho)^{1/2}}{(B/H)^{1/3}} \quad (3)$$

is a Froude number used to characterise the relative magnitudes of wind and buoyancy induced velocities. The empirical constant  $C$  is a function of entrainment into the plume (via the entrainment coefficient  $\alpha$ ) and defined as

$$C = \frac{6\alpha}{5} \left( \frac{9\alpha}{10} \right)^{1/3} \pi^{2/3}. \quad (4)$$

The change in buoyancy across the interface is represented by the reduced gravity,  $g'$ , of the upper layer where

$$\frac{g'}{G'_H} = \xi^{-5/3}. \quad (5)$$

In equation (5), the reduced gravity of the upper layer is normalised using the reduced gravity in the plume at the height  $y=H$ . The reduced gravity, or buoyancy, of the upper layer is given by

$$g' = g \frac{\Delta\rho}{\rho_1} \quad (6)$$

where  $\Delta\rho$  is the density difference between the upper and lower layers and  $\rho_1$  is a reference density (for convenience, taken to be the ambient density). Assuming the air in the space behaves as an ideal gas, equation (6) may be written in terms of the temperature difference,  $\Delta T$  and the temperature,  $T_1$ , of the ambient layer:

$$g' = -g \frac{\Delta T}{T_1}. \quad (7)$$

HL verified their analytical model using salt-bath experiments in which a Perspex box with upper and lower openings was placed in a flume of fresh water. The heat source was represented using an injection of brine. A wide range of values of  $Fr$  were investigated by varying the ‘wind’ speed in the flume and the salinity/volume flow rate of the brine. Comparison of these experimental results with the analytical predictions are shown in Figures 8-11. Note that as  $Fr$  increases the interface height descends and the buoyancy of the upper layer increases.

## SIMULATION DETAILS

### Cases Investigated

The geometry used in the CFD simulations comprised two openings at high level and two openings at low level (Figure 2). The flow was driven by a horizontal heat source in the centre of the floor and the influence of a light, steady wind (giving small  $Fr$ ) acting on the upper openings investigated. The openings were all of equal area and positioned symmetrically about a plane through the centre of the heat source. The aspect ratio of the enclosure considered is the same as that used by HL in their salt-bath experiments, although the scale is a factor of 10 greater.

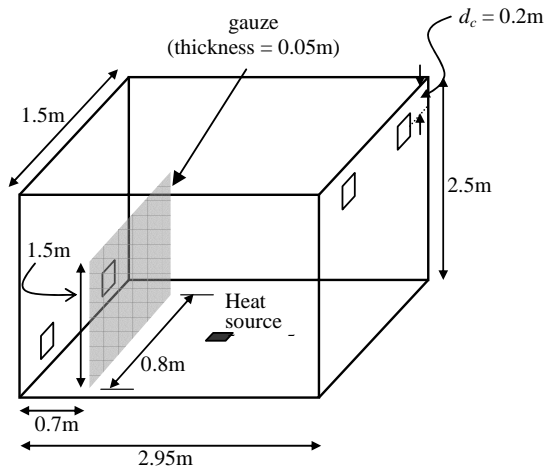


Figure 2 Geometry investigated in CFD simulations

In order to prevent the momentum of the incoming air influencing the behaviour of the buoyant plume, a fine gauze was placed between the low-level inlets and the heat source. Such a device was used both in the CFD simulations and in the salt-bath experiments.

Steady-state flows were investigated for the operating conditions shown in Table 1.

Table 1 Operating conditions for CFD simulations

OPERATING CONDITIONS	$\Delta$	$Fr$
$A^* = 0.128\text{m}^2$ or $A^* = 0.077\text{m}^2$	0	0
$Q = 100\text{W}$ ( $B = 2.75 \times 10^{-3} \text{m}^4\text{s}^{-3}$ )	0.051	2
Ambient temperature = $15^\circ\text{C}$	0.115	3
	0.205	4
	0.320	5

### CFD Model

The software used for this work was CFX4, version 4.4 (2001). This is a multiblock code in which geometries are defined using one or more topologically rectangular blocks. Each block is covered with a mesh and the governing equations are

solved using the finite volume method (Versteeg and Malalasekera, 1995).

### The Governing Equations

The code solves the following conservation equations for mass, momentum and enthalpy for a steady, incompressible turbulent flow:

$$\frac{\partial u_j}{\partial x_j} = 0 \quad (8)$$

$$\frac{\partial}{\partial x_j} (\rho u_j u_i) = \frac{\partial}{\partial x_j} \left( -p_0 \delta_{ij} + (\mu + \mu_t) \left( \frac{\partial u_i}{\partial x_j} + \frac{\partial u_j}{\partial x_i} \right) \right) + \rho g_i \quad (9)$$

$$\frac{\partial}{\partial x_j} (\rho u_j He) - \frac{\partial}{\partial x_j} \left( \left( \frac{\lambda}{C_p} + \frac{\mu_t}{\sigma_{He}} \right) \left( \frac{\partial He}{\partial x_j} \right) \right) = 0. \quad (10)$$

The Boussinesq approximation is applied in which the density in the momentum equation is written as

$$\rho = \rho_0 [1 - \beta(T - T_0)]. \quad (11)$$

The turbulent viscosity  $\mu_t$  is determined using a two-equation  $k$ - $\varepsilon$  model. Based on the findings of previous work (Cook, 1998, Cook and Lomas, 1998) the RNG  $k$ - $\varepsilon$  turbulence model of Yakhot et al. (1992) was employed. The transport equations for turbulent kinetic energy  $k$  and turbulent kinetic energy dissipation  $\varepsilon$  for this model are as follows:

$$\frac{\partial}{\partial x_j} (\rho u_j k) - \frac{\partial}{\partial x_j} \left( \left( \mu + \frac{\mu_t}{\sigma_k} \right) \frac{\partial k}{\partial x_j} \right) = P + G - \rho \varepsilon \quad (12)$$

$$\frac{\partial}{\partial x_j} (\rho u_j \varepsilon) - \frac{\partial}{\partial x_j} \left( \left( \mu + \frac{\mu_t}{\sigma_\varepsilon} \right) \frac{\partial \varepsilon}{\partial x_j} \right) = \quad (13)$$

$$(C_1 - C_{1RNG}) \frac{\varepsilon}{k} P - C_2 \rho \frac{\varepsilon^2}{k}$$

where

$$P = (\mu + \mu_t) \frac{\partial u_i}{\partial x_j} \left( \frac{\partial u_i}{\partial x_j} + \frac{\partial u_j}{\partial x_i} \right) \quad (14)$$

$$G = \frac{(\mu + \mu_t)}{\sigma_{He}} \beta g_k \frac{\partial T}{\partial x_k} \quad (15)$$

$$C_{1RNG} = \frac{\eta(1 - \eta/\eta_0)}{1 + \beta_0 \eta^3} \quad (16)$$

$$\eta = \left( \frac{P}{\mu} \right)^{1/2} \frac{k}{\varepsilon} \quad (17)$$

$\eta_0 = 4.38$ ,  $\beta_0 = 0.015$ ,  $C_1 = 1.42$  and  $C_2 = 1.68$ . The turbulent viscosity  $\mu_t$  is given by

$$\mu_t = C_\mu \rho \frac{k^2}{\varepsilon} \quad (18)$$

where  $C_\mu = 0.085$ .

The governing equations were discretised using hybrid differencing, except the mass equation where central differencing was used, and solved on a co-located grid. Pressure and velocity are coupled using the SIMPLEC technique with the Rhie-Chow interpolation algorithm (1983) to prevent decoupling due to the co-located grid. The following under-relaxation factors were used: mass  $\sim 1.0$  (no under-relaxation); momentum  $\sim 0.65$ ; enthalpy  $\sim 1.0$ ;  $k \sim 0.7$ ; and  $\varepsilon \sim 0.7$ .

To increase the stability of the solution process and aid convergence, false time-steps of 0.1s were imposed on all three momentum equations. This form of under-relaxation takes into account the time scale over which the variables evolve and the local cell size. Further details can be found in Cook (1998).

The mesh used for the CFD simulations was a hexahedral mesh comprising 68,000 elements with smaller cells located around the gauze and within the region of the thermal plume (figure 3).

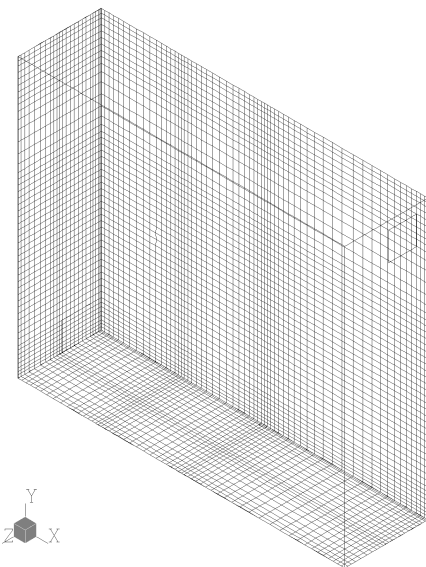


Figure 3 Hexahedral mesh structure used for CFD simulations

## Boundary Conditions

In the CFD model, only half of the geometry was modelled explicitly. This was done using a vertical symmetry plane passing through the centre of the heat source, midway between the openings. All other surfaces of the enclosure (except the heat source) were modelled as adiabatic. The heat source was represented using a constant heat flux of  $40 \text{ kW m}^{-2}$  over a source area of  $2.5 \times 10^{-3} \text{ m}^2$ .

The gauze used for absorbing momentum from the incoming air was modelled using a porous medium boundary condition which enables resistances to airflow to be imposed. Resistances were specified using a volume porosity of 0.5 together with a resistance vector of  $(300, 300, 300) \text{ Nm}^{-1}$  per  $\text{m}^3 \text{ s}^{-1}$  of flow at the level of the inlet. Above this level, the resistance was reduced to  $(150, 150, 150) \text{ Nm}^{-1}$  per  $\text{m}^3 \text{ s}^{-1}$  of flow.

At the inlet and outlet openings, constant pressures were imposed to represent the wind force. The values of pressure used were calculated such that the difference between them gave the required value of  $\Delta$  for the Froude number under consideration (Equation 3). Discussion and justification for adopting this approach to specifying boundary conditions at openings can be found in Cook et al. (2003). To account for dissipative losses and the contraction associated with the flow through the inlet and outlet openings, the physical inlet and outlet areas in the CFD model were reduced by the coefficients of expansion ( $C_e$ ) and discharge ( $C_d$ ) respectively. In this work, both coefficients take the value 0.6.

## DISCUSSION AND RESULTS

### ANALYSIS

Convergence was taken to be when the enthalpy residual (units of Watts) fell below 1% of the heat input into the space. Typically, this was achieved after about 5000 iterations.

A typical airflow pattern and typical temperature distributions are shown in figures 4-7. The velocity vectors (Figure 4) clearly show the rising plume above the heat source. This plume transports buoyant air into the upper zone of the space where a steady buoyant layer forms of uniform temperature. Figures 5-7 illustrate the increase in the depth and temperature of the upper layer as  $Fr$  increases. As the opposing wind is weak, buoyancy dominates and for the cases shown the buoyant layer is able to drive a flow out through the upper opening into the wind. Fresh ambient air enters at low level and the two-layer stratification is maintained for a range of wind speeds. These flows are qualitatively similar to those obtained for the assisting flow simulations (Cook et al. 2003). However, for given  $Fr$  and  $A^*$  values, the wind-opposed simulations predict a lower interface

height and higher temperature (reduced gravity) in the upper layer. This is in keeping with the analytical predictions and the experimental results of HL and Hunt and Linden (2001).

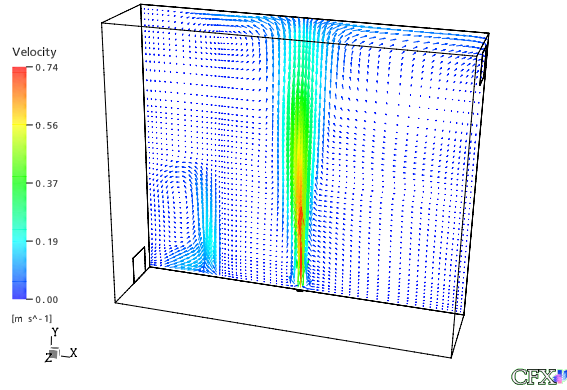


Figure 4 CFD prediction of velocity vectors  
( $A^* = 0.128\text{m}^2$ ,  $Fr = 3$ )

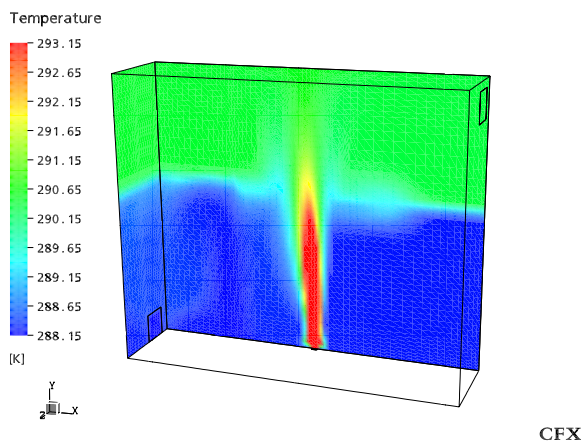


Figure 5 CFD prediction of temperature distribution  
( $A^* = 0.128\text{m}^2$ ,  $Fr = 0$ )

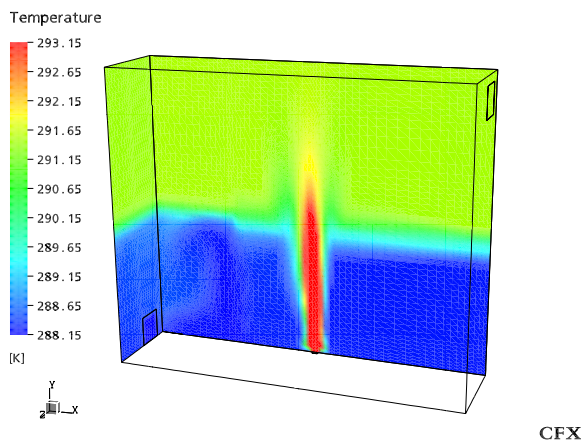


Figure 6 CFD prediction of temperature distribution  
( $A^* = 0.128\text{m}^2$ ,  $Fr = 3$ )

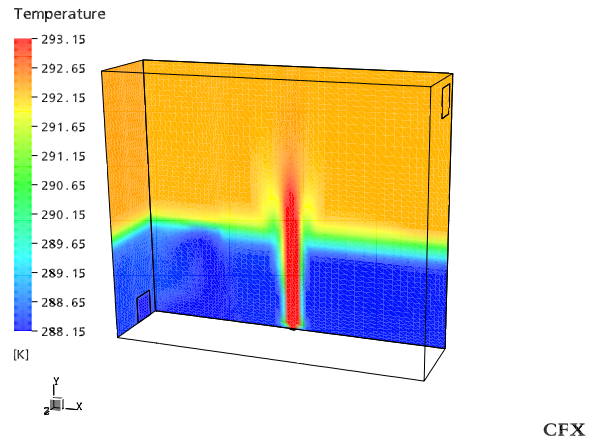


Figure 7 CFD prediction of temperature distribution  
( $A^* = 0.128\text{m}^2$ ,  $Fr = 4$ )

Quantitative results comparing the CFD predictions with the analytical and experimental work are shown in figures 8-11. Favourable agreement was achieved for the variation of interface height and reduced gravity with  $Fr$  for both  $A^*$  values investigated.

The variation of interface height with  $Fr$  shows a small over-prediction at low  $Fr$  which gradually becomes a small under-prediction as  $Fr$  increases (Figures 8 and 9). These small discrepancies may be caused by different rates of entrainment into the CFD plume compared with that assumed in the analytical work. Varying rates of entrainment may be brought about by the turbulence model employed or the performance of the gauze. Also note that the CFD predictions shown on the graph denote the mid-point of a temperature transition zone between the ambient lower layer and the warmer layer above. The variation in the extent of this transition zone varies between simulations which gives rise to a small spread in  $h/H$  values. The CFD predicted interface height for  $Fr=5$  is noticeably under-predicted (Figure 8). In this case, some inflow was observed in the simulations through the windward openings. HL show that the transition from mixing ventilation to displacement ventilation occurs when the 'internal' Froude number  $F = Fr(A^*/H^2)^{1/3} = 3^{1/2}/2^{1/3} (\approx 1.375)$ . They find that a value of  $F = F_c > 1.375$  is required to make the transition from displacement to mixing ventilation as in this case work has to be done to break down the existing thermal stratification. The parameter  $F$  is a ratio of the wind-induced and buoyancy-induced velocities *within* the enclosure and, hence, we refer to it as the 'internal' Froude number. With  $Fr=5$ ,  $A^* = 0.128\text{m}^2$  and  $H=2.5\text{m}$  we have  $Fr(A^*/H^2)^{1/3} = 1.368$  which is within 1% of  $F_c$  and, thereby, accounts for the weak inflow observed and the onset of a transition.

CFD predictions of the reduced gravity variation with  $Fr$  show a small under-prediction relative to the analytical and experimental work (Figures 10 and

11). This may again be due to differing rates of entrainment. The authors are now investigating this phenomenon by comparing the CFD-predicted plume properties (volume and buoyancy fluxes) with those determined by plume theory (Morton et al. 1956) around which the theoretical model of HL is based.

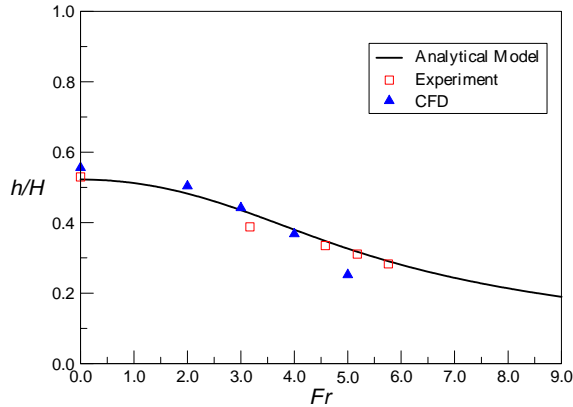


Figure 8 Variation of interface height with Froude number  $Fr$  ( $A^* = 0.128\text{m}^2$ )

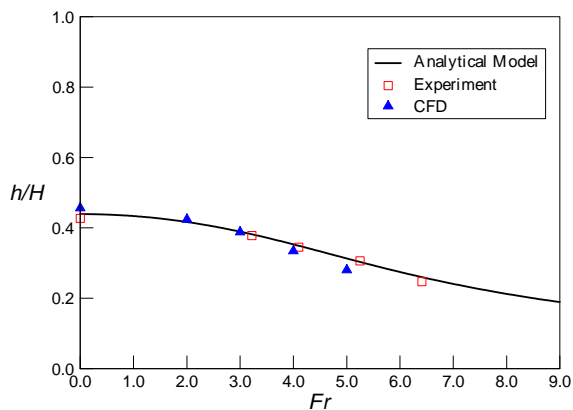


Figure 9 Variation of interface height with Froude number  $Fr$  ( $A^* = 0.077\text{m}^2$ )

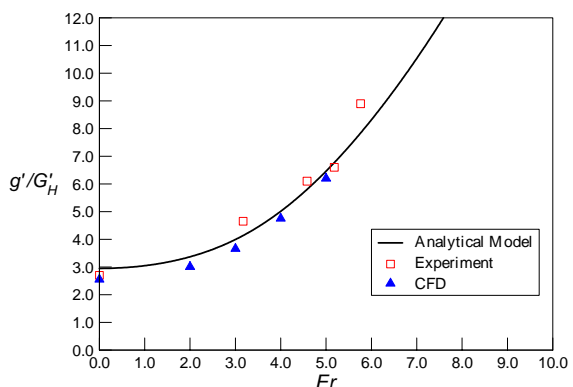


Figure 10 Variation of reduced gravity with Froude number  $Fr$  ( $A^* = 0.128\text{m}^2$ )

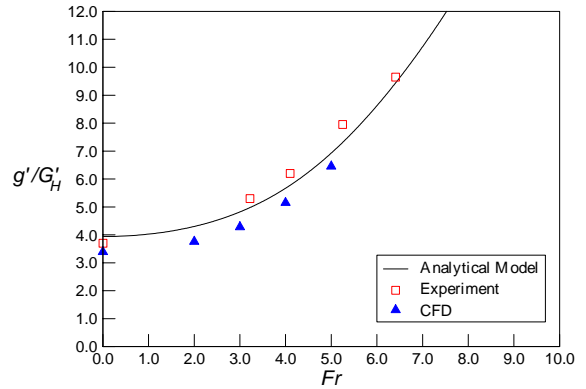


Figure 11 Variation of reduced gravity with Froude number  $Fr$  ( $A^* = 0.077\text{m}^2$ )

## CONCLUSIONS

CFD techniques have successfully been employed to model buoyancy-driven displacement ventilation in which wind forces oppose the flow. Favourable agreement was achieved in comparisons with analytical predictions and experimental measurements. Small discrepancies in the interface height separating the warm stratified air from the cooler ambient layer below are attributed to differences in the plume behaviour and performance of the gauze used for inhibiting horizontal momentum. Differences in plume structure may also be the cause of an under-prediction in the reduced gravity of the upper layer, although it should be noted that these differences are small.

A heat input, room geometry and wind pressure drop corresponding to a Froude number within 1% of the theoretical value of  $F_c = Fr(A^*/H^2)^{1/3} = 3^{1/2}/2^{1/3} (\approx 1.375)$  identified by Hunt and Linden (2005) resulted in weak inflow through the windward opening. This inflow opposed the outflowing buoyant air and signified the onset of a transition from a displacement to a mixing flow. Transitions between the flow regimes is complex and will be the subject of further CFD modelling work.

The results in this paper and those in Cook et al. (2003) will begin to form the basis for generating guidelines on how to model natural ventilation using computational fluid dynamics.

## ACKNOWLEDGMENT

The work reported here is work in progress and is part of an EPSRC supported project (GR/N37346) to establish guidelines on how best to model natural ventilation flows using CFD. The support of the EPSRC is gratefully acknowledged.

## NOMENCLATURE

$A^*$	effective opening area ( $m^2$ )
$a_L$	leeward opening area ( $m^2$ )
$a_W$	windward opening area ( $m^2$ )
$B$	source buoyancy flux ( $m^4s^{-3}$ )
$C$	empirical constant (-)
$C_1$	empirical constant (-)
$C_2$	empirical constant (-)
$C_\mu$	empirical constant (-)
$C_d$	coefficient of discharge (-)
$C_e$	coefficient of expansion (-)
$C_p$	specific heat capacity ( $J\ kg^{-1}K^{-1}$ )
$d_c$	height between top of enclosure and middle of upper opening (m)
$F$	internal Froude number (-)
$F_c$	critical internal Froude number (-)
$Fr$	Froude number (-)
$G'_H$	reduced gravity in plume at height $H$ ( $ms^{-2}$ )
$g'$	reduced gravity of warm upper layer ( $ms^{-2}$ )
$g$	acceleration due to gravity ( $ms^{-2}$ )
$H$	height of the enclosure (m)
$h$	depth of layer at ambient temperature (m)
$He$	enthalpy ( $J\ kg^{-1}$ )
$k$	turbulent kinetic energy ( $m^2s^{-2}$ )
$p_0$	'modified' pressure = $p + \frac{2}{3}\rho k - \rho_0 g_j x_j$ (Pa)
$Q$	strength of heat source (W)
$T$	temperature (K)
$T_0$	reference temperature used in CFX (K)
$u_i$	velocity vector, = ( $u, v, w$ ) ( $ms^{-1}$ )
$x_i$	position vector (m)
$\alpha$	entrainment coefficient (-)
$\beta$	coefficient of thermal expansion ( $K^{-1}$ )
$\beta_0$	empirical constant
$\Delta$	pressure drop between windward and leeward openings (Pa)
$\delta_{ij}$	Kronecker delta, = 1 if $i=j$ , = 0 if $i \neq j$
$\varepsilon$	rate of dissipation of turbulent kinetic energy ( $m^2s^{-3}$ )
$\eta_0$	empirical constant (-)
$\lambda$	conductivity ( $Wm^{-1}K^{-1}$ )
$\mu$	dynamic viscosity ( $kgm^{-1}s^{-1}$ )
$\mu_t$	turbulent (eddy) viscosity ( $kgm^{-1}s^{-1}$ )
$\rho$	air density ( $kgm^{-3}$ )
$\rho_0$	reference density used in CFX ( $kgm^{-3}$ )
$\sigma_\varepsilon$	turbulent Prandtl number for $\varepsilon$ (= 0.7179 in RNG $k$ - $\varepsilon$ model) (-)
$\sigma_{He}$	turbulent Prandtl number for enthalpy (= 0.9 in RNG $k$ - $\varepsilon$ model) (-)
$\sigma_k$	turbulent Prandtl number for $k$ (= 1.0 in RNG $k$ - $\varepsilon$ model) (-)
$\xi$	= $h/H$ , normalised interface height (-)

## REFERENCES

- CFX 2001. User Guide Version 4.4, CFX International, Harwell, UK.
- Cook, M. J. 1998. An evaluation of Computational Fluid Dynamics for Modelling Buoyancy-driven Displacement Ventilation, *PhD Thesis*, De Montfort University, Leicester, 203pp.
- Cook, M.J. and Lomas, K.J. 1998. Buoyancy-driven displacement ventilation flows: Evaluation of two eddy viscosity models for prediction, *Building Services Engineering Research and Technology*, Vol. 19, No. 1, pp.15-21.
- Cook, M. J., Ji, Y. and Hunt, G. R. 2003. CFD modelling of natural ventilation: combined wind and buoyancy forces, *International Journal of Ventilation*, Vol. 1, No. 3, pp.169-179.
- Hunt, G. R. and Linden, P. F. 2000 Multiple steady airflows and hysteresis when wind opposes buoyancy. *Air Infiltration Review*, 21, no.2, March 2000.
- Hunt, G.R. and Linden, P.F. 2001 Steady-state flows in an enclosure ventilated by buoyancy forces assisted by wind. *J. Fluid Mech.*, Vol. 426, pp. 355-386.
- Hunt, G. R. and Linden, P. F. 2005 Displacement and mixing ventilation driven opposing wind and buoyancy. *J. Fluid Mech.* Vol. 527, pp. 27-55.
- Launder, B.E. and Spalding, D.B. 1974. The numerical computation of turbulent flows, *Computer Methods in Applied Mechanics and Engineering*, Vol. 3, pp.269-289.
- Linden, P.F., Lane-Serff, G.F., and Smeed, D.A. 1990. Emptying filling boxes: the fluid mechanics of natural ventilation, *J. Fluid Mech.*, Vol. 212, pp.309-335.
- Morton, B.R., Taylor, G.I. and Turner, J.S. 1956. Turbulent gravitational convection from maintained and instantaneous sources, *Proc. R. Soc. London, A* **234**, pp. 1-23.
- Versteeg, H.K. and Malalasekera W. 1995. An introduction to Computational Fluid Dynamics – the finite volume method, Longman, New York, 257pp., ISBN 0-582-21884-5.
- Yakhot, V., Orszag, S.A., Thangham, S., Gatski, T.B. and Speziale, C.G. 1992. Development of turbulence models for shear flows by a double expansion technique, *Phys. Fluids A*, Vol. 4, No. 7, pp. 1510-1520.

